Journal of Power Sources 195 (2010) 7959–7967

Contents lists available at ScienceDirect

Journal of Power Sources

journal homepage: www.elsevier.com/locate/jpowsour

Effect of Co in the efficiency of the methanol electrooxidation reaction on carbon supported Pt

P. Hernández-Fernández [a], M. Montiel [a], P. Ocón [a], J.L.G. Fierro [b], H. Wang [c], H.D. Abruña [c], S. Rojas [b,*]

[a] Dpto. Química-Física Aplicada, Facultad de Ciencias, Universidad Autónoma de Madrid (UAM), C/Francisco Tomás y Valiente 7, 28049 Madrid, Spain
[b] Grupo de Energía y Química Sostenibles, Instituto de Catálisis y Petroleoquímica (CSIC), C/ Marie Curie 2, 28049 Madrid, Spain
[c] Department of Chemistry and Chemical Biology, Cornell University. Ithaca, NY 14853, USA

ARTICLE INFO

Article history:
Received 23 February 2010
Received in revised form 1 June 2010
Accepted 2 June 2010
Available online 22 June 2010

Keywords:
PtCo nanoparticles
Methanol oxidation reaction
DEMS
Carbon nanotubes
CO_2 efficiency

ABSTRACT

The effect of Co addition to carbon nanotubes supported Pt in the methanol oxidation reaction has been investigated by means of differential electrochemical mass spectrometry (DEMS). It has been observed that the CO_2 efficiency increases in carbon nanotubes supported PtCo compared to its homologous Pt catalysts, especially at potentials lower than 0.55 V. Despite of this, the Faradaic current reached by the bimetallic catalysts in the methanol electrooxidation was lower than those recorded on the monometallic samples. This is because Co addition difficult finding enough Pt vicinal sites for methanol dehydrogenation. On the other hand, it has been found that alloying Pt with Co, shifts down the d-band center of the larger element, so the strength of the interaction with adsorbates decreases. Consequently, it will be easier to oxidize CO_{ad} on the bimetallic surface. Furthermore, the necessary $-OH_{ad}$ species for the CO_{ad} oxidation to CO_2 will be provided by the CNTs themselves.

1. Introduction

Direct methanol fuel cells (DMFCs) have attracted great attention as power devices because of their high energy density, easy handling of methanol and their low operation temperature [1,2]. The performance of DMFCs is limited by various drawbacks, including kinetics constraints and catalyst poisoning [3,4]. In a DMFC, methanol is oxidized to carbon dioxide and water. Methanol oxidation is a slow reaction that requires active sites for the adsorption of methanol and sites that can nucleate OH_{ad} species for the oxidation of the adsorbed methanol residues [5]. Pt is the most active metal for methanol electrooxidation in acid medium. However, its performance is far from acceptable for their use as electrode in DMFCs. In this sense, bimetallic electrocatalysts such as PtRu or PtSn are more tolerant to CO poisoning while commencing methanol electrooxidation reaction at potentials less positive than bare-Pt [6–10]. However, Ru is a precious metal with an even scarcer presence than Pt [11] and with a concern toxicological effect [12]. On the other hand, Sn is not stable when subjected to potentials higher than 0.6 V vs. NHE [13]. In this context, the performance of other bimetallic alloys such as PtCo or PtNi on the methanol oxidation reaction (MOR) has been studied [14].

There is a big controversy about the performance of bimetallic PtCo catalysts in the methanol oxidation reaction. Some authors support the theory that MOR on Pt is favored by the presence of Co; however, other authors lead the opposite conclusion. Truth is that there are no clear evidences of the role of Co in the MOR.Gojkovic [15] investigated the MOR on Pt_3Co/C in acid solutions. According to their results, the rate of methanol oxidation reaction on Pt_3Co/C is not superior to that of Pt/C. In line with this study, Salgado and col. [16] found that the onset potential for MOR on PtCo/C catalysts shifted towards more positive potentials as compared to that obtained on Pt/C; that is, the presence of Co is detrimental for MOR.

Antolini et al. [14] found that the role of Co depended on its concentration. Thus, at low Co content the performance of the catalysts on the MOR is worse than that of Pt. Such effect was ascribed to the dilution effect of the active component (Pt) with a catalytically inert metal (Co) reducing methanol adsorption. However, higher contents of Co improved the performance of the catalysts on the MOR. The promotional effect was ascribed to a combination of electronic effects and to the presence of higher amounts of Co oxide species, increasing the CO oxidation.

Zeng and Lee [17] studied the catalytic activity of PtCo/C and PtCoW/C on the electrooxidation of methanol in the acidic environment of DMFCs. They found that the addition of Co promoted a more efficient initiation of methanol dehydrogenation, resulting in better catalysts for MOR in terms of Faradaic current compared to Pt/C. They also found that Pt withdraw electrons for Co atoms, increasing the amount of Pt^0 species in PtCo/C as compared to Pt/C [18].

* Corresponding author. Tel.: +34 91 585 4632; fax: +34 91 585 4760.
E-mail address: srojas@icp.csic.es (S. Rojas).

0378-7753/$ – see front matter © 2010 Elsevier B.V. All rights reserved.
doi:10.1016/j.jpowsour.2010.06.009

Table 1
Structural parameters of the electrocatalysts.

Sample	Particle size[a] (nm)	Pt (%)	Co (%)	Pt^0/Pt_{total}[b] (%)	Pt/Co[c]	EAA[d] ($m^2\ g_{Pt}^{-1}$)
PtCNT-MT	6.0	35[e]	–	63	–	32.5
PtCNT-ST	5.3	27[e]	–	61	–	58.2
PtCoCNT-MT	3.2	26[e]	10[e]	56	0.9	53.0
PtCoCNT-ST	3.6	12[e]	7[e]	68	1.1	108.3
Pt/C	3.5	40[f]	–	55	–	40.0

[a] Particle size calculated from the 220 reflection's breadth.
[b] Relative amount of reduced Pt with respect to total Pt deduced from XPS.
[c] Pt to Co atomic ratio calculated from XPS.
[d] EAA determined from the CO_{ad} stripping in $HClO_4$ media.
[e] Metallic content determined from TXRF analysis.
[f] Pt content provided by the supplier (Johnson Matthey).

These sites are responsible for the adsorption of methanol. Additionally, they proposed that $-OH_{ad}$ species are adsorbed on the Co sites, promoting methanol oxidation ("bi-functional mechanism").

On the other hand, Cui et al. [19] reported that the stabilization of $Pt–OH_{ad}$, which promotes the MOR, is favored after alloying with Co. This is because the interplanar distance and crystal lattice parameter of Pt decreased upon alloying with Co. The promotional effect of PtCo in the MOR in alkaline medium has been reported [20,21].

Lu and Reddy [22] investigated the behavior of Co–phthalocyanine–Pt/C treated at different temperatures on the MOR in acidic medium. CoPc–Pt/C treated at 980 °C exhibited the best electrochemical performance on the MOR. The superior performance on the MOR was ascribed to the presence of CoN_4 or its fragments that modify the surface of Pt. According to their study, methanol electrooxidation was more efficient and produced less intermediate organic compounds (higher CO_2 efficiency) than Pt/C. These conclusions were based on the ratio of the forward/reverse current density peaks. The higher value, the higher amount of methanol oxidized [10]. Based in similar experimental observations, Shen et al. [23] found that PtCo nanoparticles supported onto SWCNTs (single wall carbon nanotubes) showed a higher electrocatalytic activity due to a higher CO_2 efficiency in the MOR as compared to Pt/SWCNT. However, conventional electrochemical methods (cyclic voltammetry) alone are not accurate enough to establish the actual efficiency of the methanol oxidation reaction. To this end a deeper inspection of the reaction products with "operando" techniques is required. Differential electrochemical mass spectrometry (DEMS) is the ideal technique for determining the efficiency of the MOR to CO_2 or other intermediate products. To the best of our knowledge, the performance of PtCo catalysts on the MOR has only been studied by means of DEMS technique by Colmenares et al. [24]. They evaluated the activity and selectivity of Pt_3Co/C, Pt_3Ni/C and Pt/C catalysts in the MOR by means of DEMS. At 0.6, 0.7 and 0.8 V, Pt_3Co/C recorded a superior efficiency to CO_2 than Pt/C. However, those potentials are too high for DMFCs applications.

Here, we reported a comparative study of the behavior of Pt and PtCo nanoparticles supported onto multi-wall carbon nanotubes (MWCNT) in the MOR by DEMS at relevant potentials for DMFCs. Their performance is compared against a commercial Pt catalyst supported onto Vulcan XC-72R. The aim of this paper is to study the effect of Co in the mechanism of the methanol electrooxidation.

2. Experimental details

2.1. Electrocatalysts preparation

The preparation of Pt and PtCo nanoparticles was carried out using the polyol technology [25,26]. Briefly, an ethylene glycol (EG) solution of the metal precursor (Johnson Matthey H_2PtCl_6 and $CoCl_2$) was added dropwise to a suspension of the carbonaceous support (multi-wall carbon nanotubes) in EG under stirring. Previously, the carbonaceous suspension was stirred and treated in an ultrasonic bath for 30 min. The mixture was stirred for 4 h. Afterwards, a solution of NaOH (2.5 M in EG) was added to adjust the pH to 13. The total amount of water was 5 vol.%. The solution was then refluxed at 140 °C for 3 h to ensure the total reduction of the metallic precursors. This process was carried out under flowing N_2. The solid obtained was thoroughly rinsed with water and dried at 70 °C for 8 h. The most relevant physical chemical characteristics of the catalysts are compiled in Table 1.

Multi-wall carbon nanotubes (Sunnano®, purity >90%, ∅ = 10–30 nm) were used as support for the metallic nanoparticles. The functionalisation of CNTs has been carried out by means of two different methodologies. Both methods involved refluxing the multi-wall carbon nanotubes in a mixture of H_2SO_4 and HNO_3 for several hours at different temperatures. The MWCNTs obtained were designated as CNT-ST and CNT-MT in accordance with the severity of the treatment (ST, severe treatment; MT, mild treatment). The most relevant details of these procedures are summarized in Table 2.

2.2. Physico-chemical characterization

X-ray fluorescence analysis (TXRF) was performed on a Seifert EXTRA-II spectrometer equipped with two X-ray fine focus lines, Mo and W anodes, and a Si(Li) detector with an active area of 80 mm^2 and a resolution of 157 eV at 5.9 keV (Mn Kα).

X-ray diffractograms were collected on a Seifert 3000 powder diffractometer, operating with Cu Kα radiation (λ = 0.15418 nm)

Table 2
Details of the functionalisation treatment and characterization of MWCNTs.

	$[H_2SO_4:HNO_3]$ (M)	Time (h)	Temperature (°C)	%wt.[a]	O/C[b]
CNT-MT[c]	5.5:3.0	2	60	4.5	0.024
CNT-ST[d]	18.3:15.5	6	110	21.0	0.167

[a] Calculated by TGA under N_2 atmosphere.
[b] Surface atomic ratio by XPS.
[c] Mild treatment.
[d] Severe treatment.

generated at 40 kV and 40 mA. Scans at 0.02°/s for 2θ values between 10 and 90° were recorded.

X-ray photoelectron spectra (XPS) of the samples were acquired with a VG Escalab 200R spectrometer fitted with an Mg Kα ($h\upsilon$ = 1253.6 eV) 120 W X-ray source. The energy regions of the photoelectrons of interest were scanned until an acceptable signal-to-noise ratio was achieved. Intensities were estimated by calculating the integral of each peak, determined by subtraction of the Shirley type background and fitting of the experimental curve to a combination of Lorentzian and Gaussian lines of variable proportions. Accurate binding energies (±0.2 eV) were determined by referencing to the C 1s peak at 284.6 eV.

2.3. DEMS measurements

The DEMS set-up consists of two differentially pumped chambers, a quadrupole mass spectrometer (Leybold Inficon Transpector H-100M), a potentiostat (EG&G 173) and a computerized data acquisition system. The main chamber and the mass spectrometer analysis chamber were pumped by a turbomolecular pump backed by a dry diaphragm pump, in order to avoid contamination from oil vapors. The quadrupole mass spectrometer was connected to the analysis chamber and was equipped with a Channeltron Electron multiplier/Faraday cup detector with a sensitivity of 100 A $Torr^{-1}$. The time constant of the mass spectrometer was in the millisecond range.

The experimental set-up is appropriate for the simultaneous acquisition of the mass spectrometric cyclic voltammograms or chronoamperometries (MSCVs or MSCAs) for selected mass to charge ratio (m/z) and conventional CVs or CAs.

Thin-film PtCNT-ST, PtCNT-MT, PtCoCNT-MT and PtCoCNT-ST and Pt/C electrodes were prepared by pipetting 20 μL of an aqueous suspension of the catalyst onto a glassy carbon electrode (0.28 cm^2), resulting in a metal loading of 15.5 μg. The electrode was mounted into a dual thin-layer flow-through cell [27,28] and connected to the main chamber via an angle valve suited for DEMS experiments. The DEMS cell has two compartments, the upper one for electrochemical reaction and the lower one for mass spectrometric detection, which are connected through six capillaries. In the upper compartment, the working electrode was pressed against a ca. 100 μm thick Teflon spacer with an inner diameter of 6 mm, which leaves an exposed area of 0.28 cm^2 and results an electrolyte volume of 3 μL. In the lower compartment a porous Teflon membrane (Gore-Tex, 75 μm thickness, 50% porosity, 0.02 μm pore diameter) supported on a stainless steel frit served as the interface between the electrolyte and vacuum. The electrolyte flow was driven by the hydrostatic pressure in the supply bottle (flow rate about 10 μL s^{-1}), ensuring a fast transport of the species formed at the electrode to the mass spectrometric compartment. The volatile products were evaporated into the vacuum system of the DEMS (time constant ca. 1–2 s) through the porous membrane.

Two Pt wires at the inlet and outlet of the thin-layer cell, connected through an external resistance (1 MΩ), were used as the counter electrodes. A normal hydrogen electrode (NHE), connected to the outlet of the DEMS cell though a Teflon capillary, served as reference electrode.

Prior to each experiment, the electrode was cleaned in 0.1 M H_2SO_4 by cycling between 0.05 and 0.8 V at a scan rate of 50 and 10 mV s^{-1} until reproducible voltammograms were obtained.

For the study of the CO_{ad} stripping, CO was adsorbed at constant electrode potential (0.05 V) for 5 min. CO admission was accomplished by injecting 2 mL of a CO-saturated 0.1 M H_2SO_4 solution through a separate port. After CO adsorption, the cell was carefully flushed with Ar-saturated 0.1 M H_2SO_4 keeping electrode potential constant. The CO adlayer was stripped at a potential scan rate of 10 mV s^{-1}, starting at the adsorption potential and recording both Faradaic and mass spectrometric (m/z = 44) currents. Afterwards, the supporting electrolyte was exchanged with a 0.1 M H_2SO_4 solution containing 0.2 M CH_3OH and the electrode was scanned at 10 mV s^{-1}. Then, the potentiostatic measurements were carried out by means of a potential step from 0.05 V to the desired final potential where the current response was recorded during 600 s to reach the steady-state conditions (CA). Both Faradaic and mass spectrometric (m/z = 44 and m/z = 60) currents were registered.

2.4. Calibration of the DEMS set-up

For the quantitative determination of the CO_2 evolved from the methanol electrooxidation reaction a calibration experiment involving formic acid oxidation was carried out. Average current efficiencies of CO_2 formation were obtained by integrating the Faradaic charge (CV or CA) and the ion charge of m/z = 44 (MSCV or MSCA). The fraction of the charge associated to the formation of CO_2 was calculated from Eq. (1):

$$Q_F^* = 6\frac{Q_{MS}(44)}{K^*(44)} \quad (1)$$

where Q_F^* is the Faradaic charge resulting from the formation of CO_2, $Q_{MS}(44)$ is the ion charge of CO_2, 6 is the number of electrons implicated in the oxidation of methanol to CO_2 and $K^*(44)$ is the calibration constant. The value of the calibration constant was determined from the oxidation of formic acid to CO_2 [29], as shown in Eq. (2).

$$K^*(44) = 2\frac{Q_{MS}(44)}{Q_F} \quad (2)$$

where Q_F is the Faradaic charge recorded during the oxidation of formic acid to CO_2, $Q_{MS}(44)$ is the ion charge of CO_2 and 2 is the number of electrons involved in HCOOH oxidation to CO_2. Afterwards, the current efficiency for CO_2 was determined by Eq. (3):

$$A_Q = \frac{Q_F^*}{Q_F} \quad (3)$$

A_Q and Q_F accounting to the average current efficiency and to the total Faradaic charge, respectively.

3. Results and discussion

The structural parameters of the synthesized electrocatalysts are summarized in Table 1. The X-ray diffractogram of PtCNTs and PtCoCNTs samples is shown in Fig. 1. The most intense diffraction lines in the diffractograms are assigned to the fcc structure of Pt. From the shifting to higher 2θ values of the 2 2 0 and 3 1 1 diffraction lines of the Co-containing samples the formation of bimetallic PtCo particles is deduced [10]. This shifting is due to the contraction of the Pt lattice due to the incorporation of Co. The average crystallite size calculated from the Scherrer equation from the peak breadth of the 2 2 0 line lies between 5.3 and 6.0 nm for PtCNTs samples and 3.2–3.6 nm for PtCoCNTs.

XPS analysis of Pt 4f, Co 2p, C 1s and O 1s core level regions were also carried out to study the catalysts' surface. In all cases, the Pt 4f core level region displayed three doublets corresponding to Pt^0 (between 71.3 and 71.5 eV), PtO (72.8–73.3 eV) and PtO_2 (74.5–75.5 eV) species [30]. The relative amount of Pt^0 species is ca. 60% in all samples, specific details for each sample are reported in Table 1. The analysis of the Co 2p core level region of PtCoCNTs displayed three doublets at ca. 778.5, 782.2 and 785.6 eV corresponding to Co^0, CoO and Co_3O_4 species [10]. As shown in Table 1, the Pt_{at}/Co_{at} surface ratio of CNTs supported PtCo is close to 1, in good agreement with the nominal value.

The electrode active area (EAA) has been evaluated from the CO_{ad} stripping analysis recorded in 0.5 M $HClO_4$. The amount of

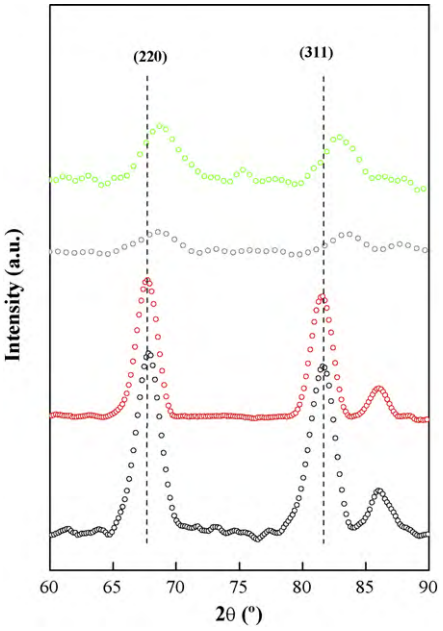

Fig. 1. Diffractograms of PtCNT-ST (black circles), PtCNT-MT (red circles), PtCoCNT-ST (green circles), PtCoCNT-MT (grey circles). (For interpretation of the references to color in this figure legend, the reader is referred to the web version of the article.)

adsorbed CO was evaluated by integration of the CO_{ad} stripping peak, corrected for the electric double-layer capacitance. The surface area was estimated assuming a monolayer of linearly adsorbed CO, its associated charge being 420 μC cm^{-2} [31]. Table 1 collects the obtained results. The electrode active area of the nanoparticles supported on CNT-ST is higher than those obtained for its homologous supported on CNT-MT. A summary with the most relevant results obtained in the physical chemical characterization for these catalysts is compiled in Table 1.

All the experiments carried out to study the methanol and CO oxidation reactions have been conducted in 0.1 M H_2SO_4 medium. The CO_{ad} stripping curve and the base voltammogram recorded on CNTs supported Pt and PtCo along with that on Pt/C are depicted in Fig. 2. According to the mass spectrometric $m/z = 44$ signal, the onset potential of CO_2 evolution is 0.3 V in CNTs supported Pt catalysts, 0.37 V in Pt/C and 0.3 and 0.37 V in PtCoCNT-ST and PtCoCNT-MT, respectively. In good agreement with previous observations [24], a CO_{ad} oxidation pre-wave is observed in the voltammograms of both PtCNT-ST and PtCNT-MT.

CO_{ad} oxidation on PtCoCNT-MT records two peaks with $Ep_{CO} = 0.73$ and 0.77 V, whereas PtCoCNT-ST records one single peak at 0.74 V. CO_{ad} oxidation is favored on the Pt nanoparticles supported on CNTs compared to the CNTs supported PtCo catalysts. According to the so-called bi-functional mechanism, CO oxidation requires the formation of $–OH_{ad}$ species [32,33]. Since PtCo particles are less oxophilic than Pt ones, the formation of $–OH_{ad}$ species, and consequently CO_{ad} oxidation is expected to be favored on Pt as compared to PtCo.

In line with the performance of the Pt and PtCo electrocatalysts in the CO oxidation reaction, a superior performance of PtCNT-ST and PtCNT-MT on the electrooxidation of methanol would be expected.

The cyclic voltammograms recorded during methanol electrooxidation on the different catalysts along with the I_{MS}–E response recorded during the formation of CO_2 ($m/z = 44$) and methylformate ($m/z = 60$) are depicted in Fig. 3. Methylformate is evolved as a result of the reaction between formic acid and methanol [27,28,34,35], its presence being indicative of the formation of formic acid and formaldehyde during the MOR. Formic acid and formaldehyde are not volatile enough to be detected in the aqueous solution via DEMS [27,35,36].

Methanol oxidation commences at potentials less positive on CNTs supported Pt than in Pt/C: 0.45 vs. 0.50 V. Furthermore, the oxidation current increases with the potential more sharply in CNTs supported Pt than on Pt/C. It may be stand out that at 0.80 V the current density on PtCNT-ST is superior to that of Pt/C. The inset to Fig. 3A represents the contribution of CO_2 formation to the total Faradaic current in one cycle. PtCNT-ST displays the highest efficiency to CO_2 of the series, amounting to 85.7%. PtCNT-MT and Pt/C record lower values, respectively 66.7% and 63.6% under the same reaction conditions. The production of methylformate ($m/z = 60$) in Pt/C is relatively important, at least as compared to that recorded on CNTs supported Pt. Considering that the Pt-based catalysts reported in this manuscript display similar Pt loadings and particle size distribution (see Table 1), the importance of the nature of the support on the electrocatalyst' performance can be inferred.

Both the Faradaic current and the efficiency to CO_2 recorded during methanol oxidation are higher on CNTs supported Pt electrocatalysts than on PtCo counterparts. Again, the support seems to play an important role on the performance of the electrocatalysts during the MOR. Thus, CNT-ST supported samples display higher efficiency to CO_2 than CNT-MT supported ones (inset to Fig. 3A).

The Faradaic current arises from the total number of exchanged electrons, which in turn is a contribution of the number of methanol molecules oxidized and the efficiency (selectivity) of the process, i.e., the number of exchanged electrons (n) per molecule. For methanol oxidation to CO_2, $n = 6$, to intermediate products, $n < 6$. Besides, the complete oxidation of methanol to CO_2 implies that less poison species remain adsorbed on the surface of the catalyst. Altogether, both features describe the performance of an electrocatalyst.

Thus far, two important conclusions can be drawn. First, Pt nanoparticles oxidize methanol more efficiently than their homologous PtCo, at least in one full potential cycle. Second, the support plays an important role in the catalytic process. Electrocatalysts prepared with carbon nanotubes containing more oxygen-bearing groups (see Table 2), PtCNT-ST and PtCoCNT-ST, display the highest efficiency to CO_2. Gómez de la Fuente et al. [30] observed that the ability of Pt/C catalysts to oxidize CO depended on the nature of the support. Also, they observed that the activity of PtRu nanoparticles in the MOR increased when these are supported in a carbonaceous material with a higher concentration of oxidized groups onto its surface, especially strong acids groups [37,38]. The same observation was extended to PtRuNi nanoparticles [39].

Fig. 4 depicts the voltammograms recorded during methanol electrooxidation in all catalysts studied in this manuscript. The Faradaic current recorded during methanol electrooxidation on Pt-based electrocatalysts is superior to that recorded on PtCo ones.

The contribution of CO_2 formation to the total Faradaic current both in the forward and in the reverse scans was evaluated by means of DEMS. Results are shown in Fig. 5. The performance of the monometallic Pt electrocatalysts in the forward and reverse scans is different. On the contrary, CO_2 production on PtCo samples is the same in the forward and reverse scans, irrespectively of the support. This similar products distribution in both scans indicates that methanol oxidation mechanism is similar when the oxides species are formed at high potentials.

The effect of the applied potential on the CO_2 formation was also studied by a series of potential step methanol electrooxidation experiments recorded at 0.50, 0.55, 0.70 and 0.80 V. Among other factors, the formation of different intermediates and products in the MOR is strongly dependent on the potential applied [40]. The methanol oxidation I_F–t curves along with the mass spectrometric currents for $m/z = 44$ and $m/z = 60$ recorded at selected potentials in Pt and PtCo supported on CNTs are shown in Fig. 6. For the sake

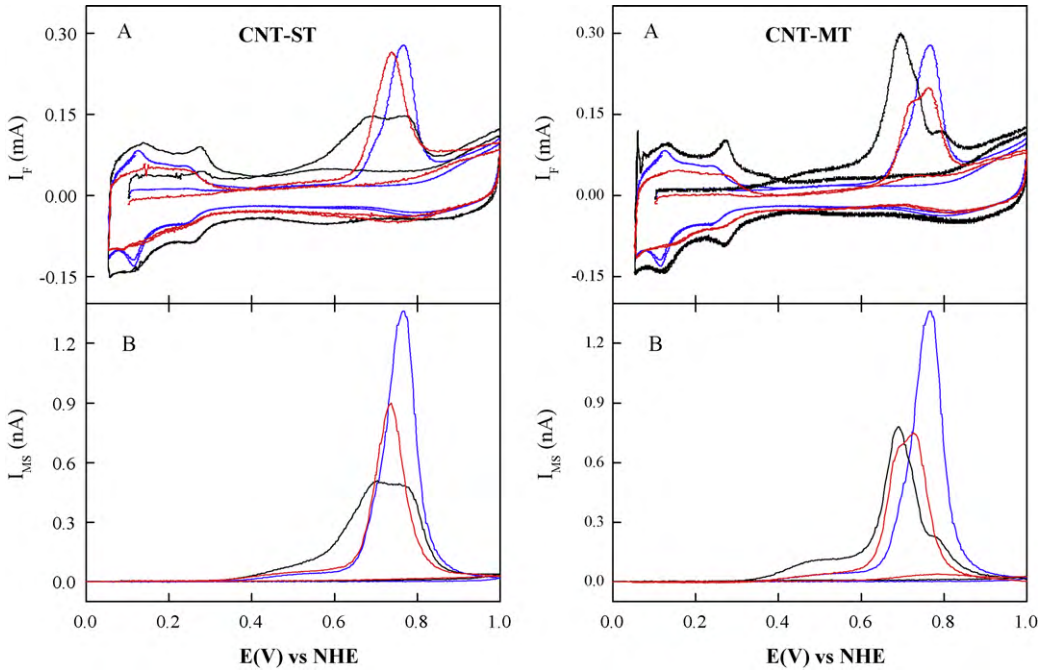

Fig. 2. Simultaneously recorded cyclic voltammetry (A) and ion current $m/z = 44$ (B) on Pt/CNTs (black), PtCo/CNTs (red) and Pt/C (blue) for the CO_{ad} oxidation. The analyses were recorded in 0.1 M H_2SO_4 at 10 mV s^{-1}. (For interpretation of the references to color in this figure legend, the reader is referred to the web version of the article.)

of comparison, the performance of Pt/C is depicted in figure. A bar diagram depicting CO_2 efficiencies recorded at these potentials is shown in Fig. 7. All catalysts display similar features in the methanol electrooxidation process. The quasy steady-state Faradaic current and the mass spectrometric current for CO_2 increased with the potential. The total Faradaic current is higher for Pt/C as compared to that recorded for Pt and PtCo supported on CNTs, except at the most positive potential (0.8 V). The Faradaic current recorded for CNTs supported Pt catalysts is higher than that of the PtCo counterparts, at least at potentials less positive than 0.8 V. Remarkably, in spite of the above mentioned trends, CNTs supported PtCo catalysts display higher efficiency to CO_2 than Pt ones, Pt/C included. This behavior is more pronounced at the less positive potentials studied, 0.50 and 0.55 V, precisely those of relevance for DMFC applications.

Compiling *I–t* data altogether, it can be concluded that CNTs supported Pt catalysts display the higher Faradaic current of the series in the methanol oxidation reaction but lower efficiency to CO_2 than CNTs supported PtCo ones. This can be rationalized by assuming that the turn over frequency (TOF) of CNTs supported Pt catalysts is higher than that of CNTs PtCo ones. A higher TOF means

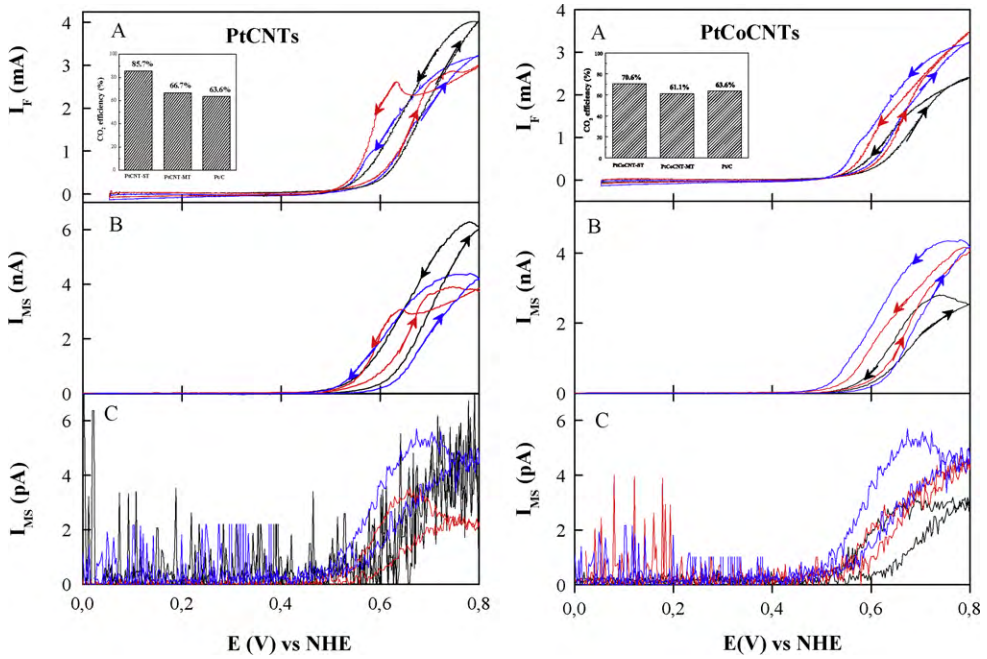

Fig. 3. Simultaneously recorded cyclic voltammetry (A) and ion current $m/z = 44$ (B) and $m/z = 60$ (C) on PtCNT-ST and PtCoCNT-ST (black line), PtCNT-MT and PtCoCNT-MT (red line) and Pt/C (blue line) for the methanol oxidation in 0.2 M Methanol + 0.1 M H_2SO_4. Scan rate: 10 mV/s. Inset Fig. 2A. CO_2 efficiencies of a full cycle. (For interpretation of the references to color in this figure legend, the reader is referred to the web version of the article.)

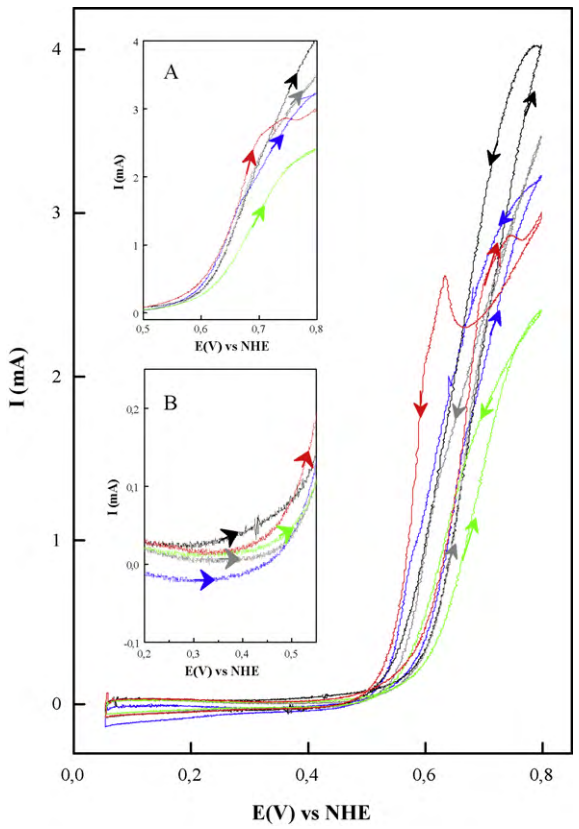

Fig. 4. Cyclic voltammetry on PtCNT-ST (black line), PtCNT-MT (red line), PtCoCNT-ST (green line), PtCoCNT-MT (grey line) and Pt/C (blue line) for the methanol oxidation in 0.2 M Methanol + 0.1 M H_2SO_4. Scan rate: 10 mV/s. Inset (A): Magnified of high potentials. Inset (B): Magnified of low potentials. (For interpretation of the references to color in this figure legend, the reader is referred to the web version of the article.)

that more methanol molecules are oxidized per active site per time unit. Remarkably, in spite of the lower Faradaic current recorded on CNTs supported PtCo catalysts in the MOR, they oxidize methanol more efficiently to CO_2 than monometallic ones. This in turn should reflect a different reaction pathway of the MOR on those catalysts. The difference performance of the bimetallic catalysts for the MOR cannot be ascribed to effects such as metal loading, particle size or Pt surface area. It should be recalled that all experiments were done using electrodes with the same amount of metal. Although the mean particle size of the bimetallic samples is similar to that of

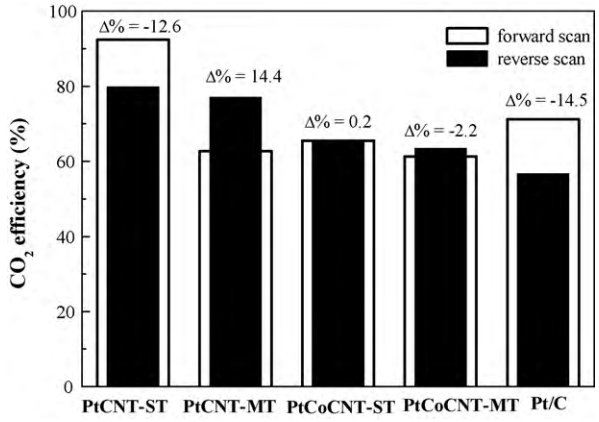

Fig. 5. CO_2 efficiencies for methanol oxidation in both forward (white) and reverse (black) scan.

Pt/C and slightly smaller than that of PtCNTs (see Table 1). A priori, the most important difference between both series of catalysts is the presence of cobalt.

It is known that by alloying platinum with ruthenium or other oxophilic metals the activity in the MOR increases due to the bifunctional character of the bimetallic material [41]. On the other hand, the higher activity of PtCo-based electrocatalysts in the oxygen reduction reaction (ORR) has been documented. Preferred explanations evoke to changes either in the lattice structure due to the alloying [42] or in the Pt–Pt interatomic distance [43,44], to the lower oxophilicity of Co, i.e., the inhibition of Pt–OH_{ad} formation on Pt sites [45–49]. This latter effect explains well the lower Faradaic current recorded on the CNTs supported PtCo catalysts during methanol electrooxidation. Another possible explanation could be related to the difficulty on finding enough Pt vicinal sites for methanol dehydrogenation due to Co dilution. It is known that methanol oxidation occurs on Pt sites through a dehydrogenation mechanism [40]. The methanol adsorption–dehydrogenation process requires at least three neighboring Pt atoms in the proper crystallographic arrangements [41,50]. The surface Pt/Co atomic ratio derived from XPS analysis is close to 1 (see Table 1), so the probability of finding three Pt sites together required to oxidizing one molecule of methanol are lower than in bare-Pt catalysts. This effect has been observed in PtAu/C samples by our group [51] and confirmed recently [52]. Furthermore, it has been found that there is lower segregation of Pt in Pt_3Co alloys, indicating a higher dilution of Pt, which causes a decrease in the number of Pt sites [53].

Different mechanisms have been proposed for the methanol oxidation reaction. Bagotzki et al. [5] suggested that the reaction involves successive dissociations of C–H bonds, followed by the formation of CO_2 or intermediates products such as formaldehyde, CO, formic acid, and methylformate. Davis and Barteau [54] suggested that the reaction starts with the scission of the O–H bond, followed by different dissociations of C–H bonds. Notwithstanding the actual mechanism of the MOR, the first step should be the adsorption of methanol on the Pt surface. The role of Co in terms of the dilution effect has been discussed above; however, this is not the only effect of Co.

It has been found that the addition of Co to a matrix of Pt decreases the interaction with molecules like CO, NO or O_2. Variations in the surface electronic structure for pseudomorphic overlayers and impurities of different metals like Au, Co, Pt, Ru, Pd, etc., on other metals have been studied by Ruban et al. [55]. By knowing these variations, trends in the reactivity of metal surfaces can be deduced. They studied the importance of variations in the center of d-bands, which produces changes in the adsorption and activation energies from one metal to the next. They concluded that when the small elements in the periodic table (smaller Wigner–Seitz radius) are alloyed into or put on the top of the larger elements, their d-band center shifts up in order to maintain the same d-band filling locally. In parallel and due to the same explanation, the d-band center of the large element (larger Wigner–Seitz radius) shifts down. Consequently, the strength of the interaction between the adsorbate and the smaller element increases. On the contrary, a lower adsorption energy value is found between the element with the larger radius and the adsorbate. In our context, this effect results in a decrease of the adsorption energy of CO on Pt sites in the CNTs supported PtCo catalysts with respect to the monometallic samples. Consequently, it will be easier to oxidize CO_{ad} on such a bimetallic surface and the CO_2 efficiency should be higher than in the platinum samples (see Figs. 4 and 6). Other factor to have into account is the generation of –OH_{ad} species on the CNTs. It is known that CNTs defect with high reactivity are easily oxidized to oxygen-containing groups at low potentials [56,57]. The required potential to this oxidation decreases due to the presence of tran-

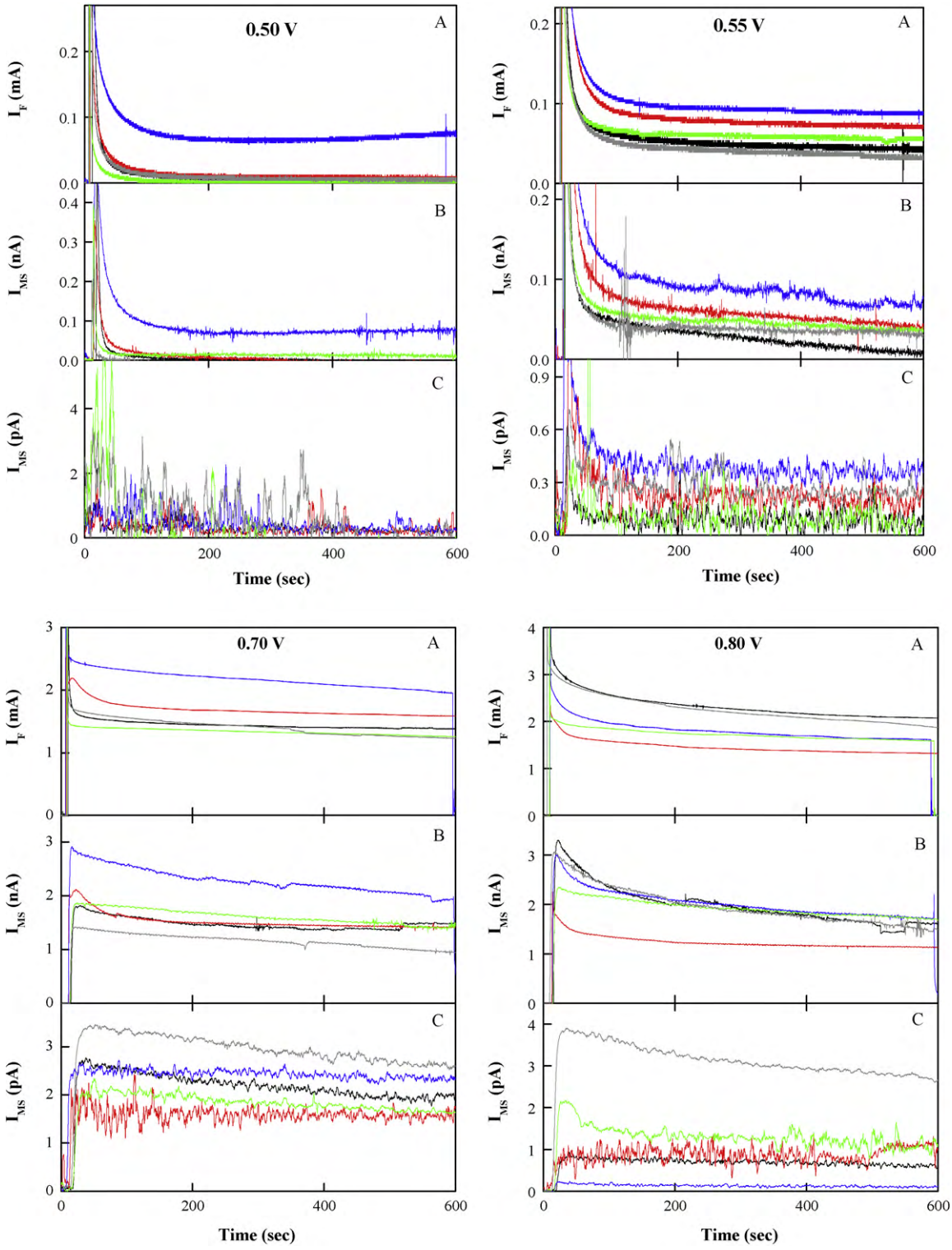

Fig. 6. Simultaneously recorded cronoamperommetry (A) and ion current $m/z = 44$ (B) and $m/z = 60$ (C) on PtCNT-ST (black line), PtCoCNT-ST (green line), PtCNT-MT (red line), PtCoCNT-MT (grey line) and Pt/C (blue line) for the methanol oxidation in 0.2 M methanol + 0.1 M H_2SO_4. Step potential from 0.05 to 0.50, 0.55, 0.70 and 0.80 V (600 s per potential). (For interpretation of the references to color in this figure legend, the reader is referred to the web version of the article.)

sition metals [58]. So, even if in principle $-OH_{ad}$ formation will be impeded by the presence of Co, the CNTs can be by themselves the source of such $-OH_{ad}$ species necessary for the CO_{ad} oxidation to CO_2.

Relevant aspects of the methanol electrooxidation on Pt electrodes, pertinent to the discussion in here, have been disclosed by Iwasita [6] by means of voltammetry and spectroscopic measurements. Thus, in spite of the higher production of CO_2 originated on Pt (1 1 0) compared to Pt (1 1 1), the Faradaic current during the MOR was lower in the former. She concluded that in the interval of potentials between ca. 0.4 and 0.6 V, the Pt (1 1 1) surface originates a large extent of species from the dissociative adsorption of methanol and/or from parallel pathways ending in products other than CO_2. CNTs supported Pt catalysts produced high Faradaic

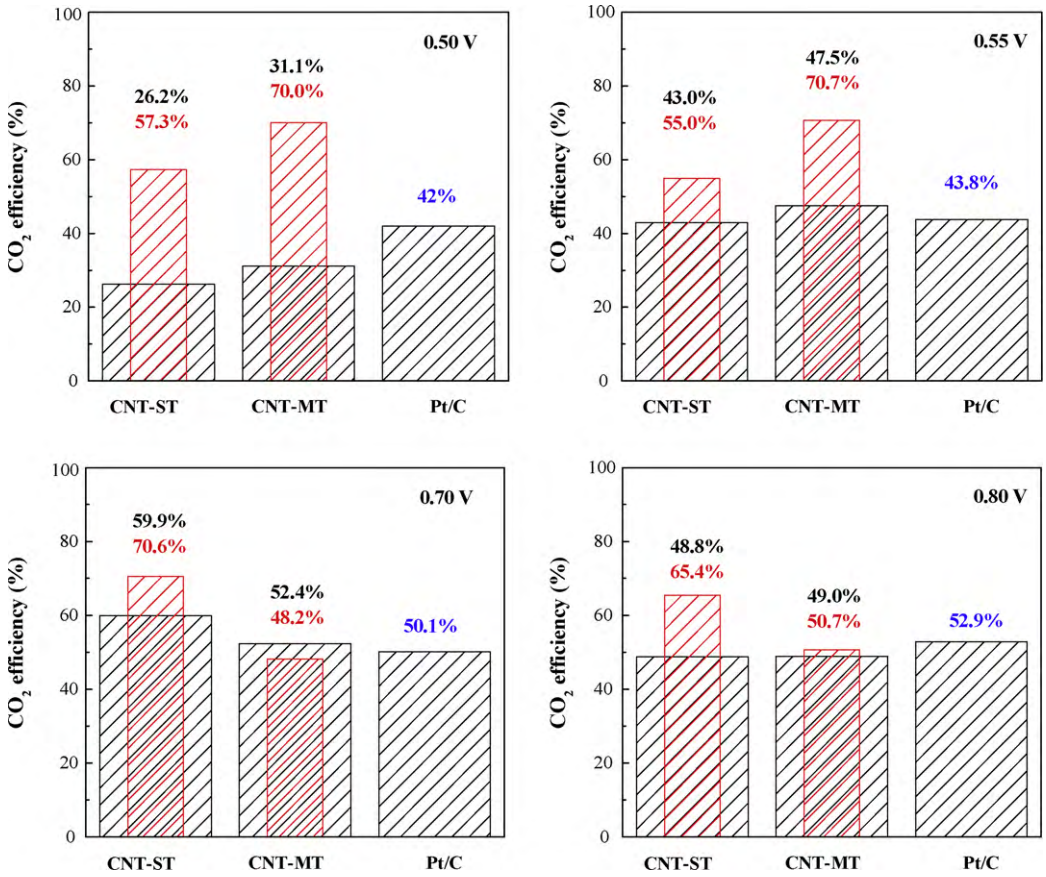

Fig. 7. CO_2 efficiencies for methanol oxidation after a potential step from 0.05 to 0.50, 0.55, 0.60, 0.70 and 0.80 V. PtCNTs (black), PtCoCNTs (red) and Pt/C (blue). (For interpretation of the references to color in this figure legend, the reader is referred to the web version of the article.)

oxidation current, including both the total oxidation of methanol to CO_2 and to other intermediate products. The MOR is favored onto these surfaces due to a higher facility to find the necessary Pt atoms for the methanol dissociative adsorption to occur. On a Pt surface, a larger amount of these sites are available, so more methanol molecules become oxidized, at least partially.

In the chronoamperommetry recorded at 0.80 V (Fig. 6), the Faradaic current for the MOR depicts the following trend: PtCNT-ST ≥ PtCoCNT-MT > Pt/C ≥ PtCoCNT-ST > PtCNT-MT. The lower Faradaic current reached by the PtCNT-MT catalysts is probably related with the oxide formation at high potentials. As shown in Fig. 5, this process affects severely to the Pt-based catalysts, which change their MOR mechanism.

4. Conclusions

The effect of Co addition over the activity of the methanol oxidation reaction has been studied in CNTs supported Pt electrocatalysts. It has been demonstrated that the mechanism of the reaction is not influenced by the formation of metal oxides species in the CNTs supported PtCo catalysts. The CO_2 efficiencies are clearly superior in the bimetallic samples, especially at lower potentials (0.50 and 0.55 V), region of great interest for the methanol oxidation reaction. This fact is related with the decrease in the CO adsorption energy due to the shift of the d-band center, which facilitates its ulterior oxidation. The lower Faradaic current obtained in the bimetallic samples is due to the lower possibility of finding enough Pt sites together for methanol dehydrogenation due to Co dilution.

With respect to the role of the support, carbon nanotubes could provide –OH species which help in the CO_{ad} oxidation to CO_2. The nanoparticles supported onto the CNTs with a larger amount of oxygen-containing groups (CNT-ST) have displayed the highest CO_2 efficiencies, at least in the cyclic voltamperometric studies.

Acknowledgments

P. Ocón acknowledges to CICyT project reference CTQ-2007-66547/BQU for financial support. M. Montiel thanks the CAR for a grant. S. Rojas acknowledges to the CSIC-CAM project reference 200680M013 for financial support. This material is based upon work supported as part of the Energy Materials Center at Cornell (EMC^2), an Energy Frontier Research Center funded by the U.S. Department of Energy, Office of Science, Office of Basic Energy Sciences under Award Number DE-SC0001086.

References

[1] R. Dillon, S. Srinivasan, A.S. Arico, V. Antonucci, J. Power Sources 127 (2004) 112.
[2] G. Apanel, E. Jonson, Cells Bull. 11 (2004) 12.
[3] A.J. Appleby, F.R. Foulkes, in: Van Remhold (Ed.), Fuel Cell Handbook, New York, 1989.
[4] S. Gottesfeld, T.A. Zawodzinski, in: R.C. Alkire, H. Gerisher, D.M. Kolb, C.W. Tobias (Eds.), Advances in Electrochemical Science and Engineering, VCH, Weiheim, 1997.
[5] V.S. Bagotzki, Y.B. Vassiliev, O.A. Kazova, J. Electroanal. Chem. 81 (1977) 229.
[6] T. Iwasita, Electrochim. Acta 47 (2002) 3663.
[7] R. Parsons, T. VanderNoot, J. Electroanal. Chem. 257 (1988) 9.
[8] S. Wasmus, A. Kuver, J. Electroanal. Chem. 461 (1999) 14.
[9] H.A. Gasteiger, N. Markovic, P.N. Ross Jr., E.J. Cairns, J. Phys. Chem. 97 (1993) 12020.
[10] M. Montiel, P. Hernández-Fernández, J.L.G. Fierro, S. Rojas, P. Ocón, J. Power Sources 191 (2009) 280.
[11] T. Okada, Y. Suzuki, T. Hirose, T. Ozawa, Electrochim. Acta 49 (2004) 385.

[12] T. Ioroi, K. Yasuda, Z. Siroma, N. Fujiwara, Y. Miyazaki, J. Electrochem. Soc. 150 (2003) A1225.
[13] K. Wang, H.A. Gasteiger, N.M. Markovic, P.N. Ross Jr., Electrochim. Acta 41 (1996) 2587.
[14] E. Antolini, J.R.C. Salgado, E.R. González, Appl. Catal. B: Environ. 63 (2006) 137.
[15] S.L.J. Gojkovic, J. Serb. Chem. Soc. 68 (2003) 859.
[16] J.R.C. Salgado, E. Antolini, E.R. Gonzalez, Appl. Catal. B: Environ. 57 (2005) 283.
[17] J. Zeng, J.Y. Lee, Int. J. Hydrogen Energy 32 (2007) 4389.
[18] J. Zeng, J.Y. Lee, J. Power Sources 140 (2005) 268.
[19] Z. Cui, J. Shi, L. Zhang, M. Ruan, J. Gao, Carbon 47 (2009) 186.
[20] X. Zhang, K.-Y. Chan, J. Mater. Chem. 12 (2002) 1203.
[21] X. Zhang, K.-Y. Tsang, K.-C. Chan, J. Electroanal. Chem. 573 (2004) 1.
[22] Y. Lu, R.G. Reddy, Int. J. Hydrogen Energy 33 (2008) 3930.
[23] J. Shen, Y. Hu, C. Li, C. Qin, M. Ye, Electrochim. Acta 53 (2008) 7276.
[24] L. Colmenares, E. Guerrini, Z. Jusys, K.S. Nagabhushana, E. Dinjus, S. Behrens, W. Habicht, H. Bönnemann, R.J. Behm, J. Appl. Electrochem. 37 (2007) 1413.
[25] D. Larcher, R. Patrice, J. Solid State Chem. 154 (2000) 405.
[26] W. Li, C. Liang, W. Zhou, J. Qiu, Z. Zhou, G. Sun, Q. Xin, J. Phys. Chem. B 107 (2003) 6292.
[27] H. Wang, T. Loeffler, H. Baltruschat, J. Appl. Electrochem. 31 (2001) 759.
[28] H. Wang, C. Wingender, H. Baltruschat, M. López, M.T. Reetz, J. Electroanal. Chem. 509 (2001) 163.
[29] H. Wang, L. Alden, F.J. DiSalvo, H.D. Abruña, Phys. Chem. Chem. Phys. 10 (2008) 3739.
[30] J.L. Gómez de la Fuente, S. Rojas, M.V. Martínez-Huerta, P. Terreros, M.A. Peña, J.L.G. Fierro, Carbon 44 (2006) 1919.
[31] X. Xue, T. Lu, C. Liu, W. Xu, Y. Su, Y. Lv, W. Xing, Electrochim. Acta 50 (2005) 3470.
[32] T. Yajima, N. Wakabayashi, H. Uchida, M. Watanabe, Chem. Commun. (2003) 828.
[33] A. Kabbabi, R. Faure, R. Durand, B. Bedan, F. Hahn, J.-M. Leger, C. Lamy, J. Electroanal. Chem. 444 (1998) 41.
[34] T. Iwasita, W. Vielstich, J. Electroanal. Chem. 201 (1986) 10874.
[35] Z. Jusys, R.J. Behm, Electrochim. Acta 49 (2004) 3891.
[36] Z. Jusys, J. Kaiser, R.J. Behm, Langmuir 19 (2003) 6759.
[37] J.L. Gómez de la Fuente, M.V. Martínez-Huerta, P. Terreros, J.L.G. Fierro, M.A. Peña, Catal. Today 116 (2006) 422.
[38] J.L. Gómez de la Fuente, M.V. Martínez-Huerta, P. Terreros, J.L.G. Fierro, M.A. Peña, Carbon 43 (2005) 3002.
[39] M.V. Martínez-Huerta, S. Rojas, J.L. Gómez de la Fuente, P. Terreros, M.A. Peña, J.L.G. Fierro, Appl. Catal. B: Environ. 69 (2006) 75.
[40] J.L. Cohen, D.J. Volpe, H.D. Abruña, Phys. Chem. Chem. Phys. 9 (2007) 49.
[41] H.A. Gasteiger, N. Markovic, P.N. Ross Jr., E.J. Cairns, Electrochim. Acta 39 (1993) 1825.
[42] S. Mukerjee, S. Srinivasan, J. Electroanal. Chem. 357 (1993) 201.
[43] Q. Huang, H. Yang, Y. Tang, T. Lu, D.L. Akins, Electrochem. Commun. 8 (2006) 1220.
[44] S. Mukerjee, M.P. Srinivasan, M.P. Soriaga, J. McBreen, J. Phys. Chem. 99 (1995) 4577.
[45] V. Stamenkovic, T.J. Schmidt, P.N. Ross, N.M. Markovic, J. Phys. Chem. 106 (2002) 11970.
[46] V. Stamenkovic, T.J. Schmidt, P.N. Ross, N.M. Markovic, J. Electroanal. Chem. 554 (2003) 191.
[47] A.S. Arico, A.K. Shukla, H. Kim, S. Park, M. Min, V. Antonucci, Appl. Surf. Sci. 172 (2001) 33.
[48] J.K. Norskov, J. Rossmeisl, L. Al Logadottir, J.R. Lindqvist, T. Kitchin, H. Bligaard, Jonsson, J. Phys. Chem. B 108 (2004) 17886.
[49] F.H.B. Lima, W.H. Lizcano-Valbuena, E. Teixeira-Neto, F.C. Nart, E.R. González, E.A. Ticianelli, Electrochim. Acta 52 (2006) 385.
[50] C. Lamy, A. Lima, V.Le. Rhun, C. Countanceau, J.M. Leger, J. Power Sources 105 (2002) 283.
[51] P. Hernández-Fernández, S. Rojas, P. Ocón, A. de Frutos, J.M. Figueroa, P. Terreros, M.A. Peña, J.L.G. Fierro, J. Power Sources 177 (2008) 9.
[52] G. Selvarani, S.V. Selvaganesh, S. Krishnamurthy, G.V.M. Kiruthika, P. Sridhar, S. Pitchumani, A.K. Shukla, J. Phys. Chem. C 113 (2009) 7461.
[53] U.B. Demirci, J. Power Sources 173 (2007) 11.
[54] J.L. Davis, M.A. Barteau, Surf. Sci. 235 (1990) 235.
[55] A. Ruban, B. Hammer, P. Stoltze, H.L. Skriver, J.K. Norskov, J. Mol. Catal. A: Chem. 115 (1997) 421.
[56] J. Chen, M. Wang, B. Liu, Z. Fan, K. Cui, Y. Kuang, J. Phys Chem. B 110 (2006) 11775.
[57] C.-T. Hsieh, J.-Y. Lin, J. Power Sources 188 (2009) 347.
[58] Y. Shao, G. Yin, Y. Gao, P. Shi, J. Electrochem. Soc. 153 (2006) 1093.